Azimuthal extents of field variations and energetic particle source regions during a sawtooth event

S. Kasahara,[1,2] Y. Miyashita,[1] T. Takada,[1] M. Fujimoto,[1] V. Angelopoulos,[3]

H. U. Frey,[3] J. Bonnell,[4] J. P. McFadden,[4] D. Larson,[4] U. Auster,[5] and I.

Mann[6]

S. Kasahara, Institute of Space and Astronautical Science, JAXA, Sagamihara, Kanagawa 229-8510, Japan. (kshr@stp.isas.jaxa.jp)

[1]Institute of Space and Astronautical

Multi-satellite and ground-based observations show the difference between the azimuthal extents of field and energetic particle variations at the beginning of a so-called “sawtooth” event. In a few min after the substorm onset, dipolarizations at geosynchronous orbit and intensifications of positive/negative bays on the ground were observed from dusk to dawn sectors, while dispersionless flux enhancements of energetic particles occurred in a narrower longitudinal range. The timings and locations of dispersionless flux enhancements were different between electrons and ions, suggesting that their source regions were not common in this event. Although the convective (duskward)

Science, JAXA, Sagamihara, Kanagawa, Japan.

[2]The University of Tokyo, Bunkyo, Tokyo, Japan.

[3]University of California, Los Angeles, California, USA.

[4]University of California, Berkeley, California, USA.

[5]Technical University of Braunschweig, Braunschweig, Germany.

[6]University of Alberta, Edmonton Alberta, Canada.

electric field was observed by THEMIS, the energetic particle injection from the tail was not observed at the location.

1. Introduction

Quasiperiodic oscillations of energetic particle flux (EPF), the so-called sawtooth event, was first identified by *Belian et al.* [1995]. The recurrent flux variations have a periodicity of 2-4 hours and can last more than five cycles [*Borovsky et al.*, 2003; *Huang et al.*, 2003a, 2003b]. Each "tooth" consists of a sharp flux increase and a subsequent gradual decrease near the geosynchronous region, associated with dipolarization. Although such EPF variations can be also seen during isolated substorms, there is some debate on whether sawtooth events are the quasi-periodic substorms or some other kind of disturbances [*Lee et al.*, 2004; *Henderson et al.*, 2006a].

The most significant phenomenological difference between the sawtooth events and isolated substorms is that the former has larger longitudinal extents of dipolarization [*Cai et al.,* 2006], substorm current wedge (SCW) [*Kitamura et al.,* 2005], and EPF increase [*Henderson et al.,* 2006b]. From such building blocks, one may construct the likely scenario: the duskward electric field is induced over the broad azimuthal range by the broad SCW and dipolarization, and causes energetic particle injection from the tail over the large longitudinal range.

However, the relationship between azimuthal extents of dipolarization and energetic particle "source regions" in a few min after the onset has not been confirmed by observations. Note that here we define the "source region" as the region where the dispersionless flux increase over the pre-substorm flux level occurs; EPF enhancements outside the source region show energy dispersions, since they are the results of curvature/gradient drift. Furthermore, the equatorial electric field, which should play an important role in particle injections from the tail, has rarely been observed during sawtooth events, due to the lack of the electric field instruments.

In the present paper, we report the difference between the azimuthal extents of electromagnetic fields and energetic particle source regions during the first "tooth" (EPF variation) of a sawtooth event. Even though the tooth might be different from isolated substorms, we call it substorm hereafter, just for convenience.

2. Observations

2.1. Instrumentation

THEMIS is a constellation of five satellites [*Angelopoulos et al.*, 2008]. Each satellite has an equatorial orbit and observes the inner magnetospheric region on every pass. We used energetic particle flux data (> 25 keV) obtained by the Solid State Telescope (SST) [*Larson et al.*, 2008], electric field data obtained by the Electric Field Instrument (EFI) [*Bonnell et al.*, 2008], and magnetic field data obtained by the Fluxgate Magnetometer (FGM) [*Auster et al.*, 2008]. Moments calculated from particle data obtained by the Electrostatic Analyzers (ESAs) [*McFadden et al.,* 2008] were also used.

The LANL satellites observe energetic particles ($>\sim$50 keV) with the SOPA [*Belian et al.*, 1992], while the GOES satellites measure the magnetic field.

2.2. Substorm Onset: Ground Observations

In the present study, we focus on the substorm event, which corresponds to the first "tooth" during a sawtooth event on 20 November 2007. Geomagnetic field variations observed from THEMIS Ground Based Observatory (GBO) [*Mende et al.*, 2008] and some other stations are shown in Figure 1. Small magnetic negative bays at high latitudes and positive bays at mid/low latitudes were first observed at 09:04:30 UT, followed by the intensification at $\sim$ 09:08:30 UT as indicated by large negative/positive bays. They were observed almost simultaneously over a broad longitudinal range (at least $\sim$17.5 to 4.5 hours MLT).

2.3. In Situ Observations

The satellite orbits in GSM coordinates during 8 to 10 UT are shown in Figure 2. The LANL satellites were located at the dusk (LANL-97A, L97 hereafter), midnight (1989-046, L89), and dawn (1994-084, L94) sectors. GOES-11 (G11) and GOES-12 (G12) were at the midnight and dawn sectors, respectively. THEMIS-C (THC) was on outbound pass and at the postmidnight sector. Other THEMIS satellites were not located near the nightside geosynchronous region. In the x-z plane of Figure 2, the model magnetic fields [*Tsyganenko*, 2002a, 2002b] on the THC pass are illustrated for 09:00, 09:10, and 09:20 UT. The input parameters were tuned for each time to reproduce the measured magnetic fields. In the right panels of Figure 2, ion flows perpendicular to the background magnetic field are represented by arrows, in every 10 min from 8 to 10 UT, and in every 1 min for the period of bursty flows (09:00-09:15 UT). The positive v_x and negative v_z correspond to the inward (earthward) flow in terms of the magnetic shell. The observed ion flows are almost identical to the $\mathbf{E}\times\mathbf{B}$ drift velocities, as shown in Figures 3a-c. Here we assumed $\mathbf{E}\cdot\mathbf{B} = 0$ to obtain E_z in the spacecraft frame.

Figure 3d presents magnetic field variations at G11 (MLT $\sim$0.5 h), THC (MLT $\sim$2.5 h), and G12 (MLT $\sim$4.5 h). The elevation angles, $\arctan(|B_V/B_H|)$, are plotted as a measure of dipolarization. Here we used VDH coordinates; H is anti-parallel to the Earth's dipole axis (positive northward), D denotes the azimuthal direction (positive eastward), and V completes the orthogonal coordinates and is positive outward from the center of Earth. THC (MLT ~2.5 h) observed the dipolarization at 09:05 UT (30 s after the substorm onset), simultaneously with the inward bursty flow initiation (the black solid line in Figure 3). Similarly, G11 (MLT ~0.5 h) detected the initiation of magnetic field change at 09:05 UT and then observed the intensification of dipolarization at 09:08:30 UT, simultaneously with the ground observations. G12 (MLT ~ 4.5h) also detected a slight increase in the elevation angle after the substorm onset.

Figures 3e and 3f show EPF variations for ions (~140 keV) and electrons (~130 keV), respectively. The data from the three LANL satellites and THC are displayed. The THC flux increase started around 09:05 UT, and was temporarily suspended with the intermission of the dipolarization (09:07:30-09:10:00). At around 09:10 UT, the electron flux significantly enhanced, compared to the pre-substorm level (~5×10^2 cm^{-2} sr^{-1} keV^{-1} s^{-1} for ~130 keV; L89 and L94 have continued to observe this flux level for > 1 hour prior to the onset), while the ion flux showed no significant enhancement compared to the pre-substorm level of ~100 cm^{-2} sr^{-1} keV^{-1} s^{-1} for ~140 keV ions observed by L89 and L94. L89 (MLT ~0 h) observed both ion and electron enhancements over the pre-substorm levels. At the location of L97 (MLT ~19 h), the electron flux recovered to the pre-substorm level without a net increase, while the ion flux enhanced over the pre-substorm level. L94 in the dawn sector observed gradual flux enhancement of electrons, which shows energy dispersion (not shown). These observations are summarized in Table 1.

3. Discussion

3.1. Longitudinal Extent of Dipolarization

G11 (MLT ∼0.5 h), THC (MLT ∼2.5 h), and G12 (MLT ∼4.5 h) observed the dipolarization at or around the substorm onset. Furthermore, the sudden EPF recovery at L97 (MLT ∼19 h) to the pre-substorm level can be regarded as the result of the dipolarization at the location [cf., *Clauer et al.*, 2006]. These observations indicate that the dipolarization expanded in a few min over the broad longitudinal range (at least from ∼19 to ∼4.5 hours MLT). The positive/negative bays on the ground (from ∼17.5 to 4.5 hours MLT) also support the picture.

3.2. Longitudinal Extent of the Energetic Particle Source

After the intensification of the dipolarization at 09:08:30 UT, the energetic ion fluxes started to increase at L97 (MLT ∼19 h) and L89 (MLT ∼0 h), as shown in Figure 3e. We regard these flux increases as "enhancement", since there were net increases over the pre-substorm levels, unlike, for example, the electron flux "recovery" at L97 (MLT ∼19 h). On the other hand, neither THC (MLT ∼2.5 h) nor L94 (MLT ∼6 h) observed significant enhancement of the ion flux until after ∼09:20 UT. THC observed only the recovery to the pre-substorm level associated with the dipolarization. The same features are seen in different energy channels greater than ∼80 keV (not shown). These observations indicate that the eastward edge of the source region of energetic ions was between L89 (MLT ∼0 h) and THC (MLT ∼2.5 h).

The electron flux enhancements were seen at L89 (MLT ∼0 h), THC (MLT ∼2.5 h), and L94 (MLT ∼6 h) after the initiation of dipolarization (Figure 3f). Since the L97 electron flux level was maintained at the pre-substorm level, the westward edge of the electron source region was considered to be between L97 (MLT ∼19 h) and L89 (MLT ∼0 h). It should be noted that the significant electron flux enhancements at L89 (MLT ∼0 h) and THC (MLT ∼2.5 h) started at ∼09:10 UT; there is a delay of a few min after the ion flux enhancement at L97 (MLT ∼19 h) and L89 (MLT ∼0 h). One possibility of the delay is that the eastward edge of the electron source region was far westward of L89 (MLT ∼0 h). If this is the case, the eastward edge of the electron source region was more westward than that for ions; this is contrary to the model suggested by *Birn et al.* [1997] for isolated substorms. An alternative idea is that the electron source region appeared at L89 (MLT ∼ 0 h), but with a time delay of a few min after the ion flux enhancement.

In any case, the eastward edge of the electron source region was westward of THC, since the thermal electrons at THC did not significantly change with the energetic electrons (not shown here); it indicates that the enhancement of the energetic electron flux after the intensification at THC was due to the curvature/gradient drift motions. Furthermore, again in any case, it is suggested that the source region is not common for electrons and ions, but exists separately, as known for isolated substorms [*Birn et al.*, 1997].

3.3. Role of Convection Electric Field

The earthward flows (i.e., the positive v_x and negative v_z) were observed by THC from ∼09:05 to 09:15 UT. The earthward velocity is comparable to azimuthal velocity of the curvature/gradient drift of 100 keV particles in the dipole field. Thus, one might think that the trajectories of energetic particles were significantly deflected earthward, and the particles were injected from the tail into the geosynchronous orbit in this period.

However, as shown in Figure 3 and discussed in the previous subsection, the THC EPFs only recovered to the pre-substorm levels at the first earthward flow that started at 09:05 UT. Although the electron flux enhanced after the second bursty flow that started at ∼09:10 UT, the enhancement is interpreted as the consequence of curvature/gradient drift, rather than the direct injection from the tail. Furthermore, the ion flux remained at the pre-substorm level. This may be due to a much faster azimuthal drift velocity in sawtooth events than usual [cf., *Pulkkinen et al.*, 2006]. We also have the possibility that the observed electric field was localized in a too small region to inject energetic particles from the tail.

4. Summary

We examined the simultaneous observations of electromagnetic fields and energetic particle fluxes by THEMIS-C at the nightside with the aid of geosynchronous satellites and ground stations such as THEMIS GBO. As summarized in Table 1, we found that the dipolarization expanded over the broad azimuthal range, while dispersionless EPF enhancements in a few min after the dipolarization occurred in a narrower longitudinal range. Although the inward (earthward, in terms of the magnetic shell) $\mathbf{E}\times\mathbf{B}$ drift of low energy particles was observed by THC during the dipolarization period, the injection of energetic particles from the tail was not seen at the location. Multipoint, full set observations of THEMIS, with more suitable alignments (e.g., another THEMIS satellite around 21 hours MLT in this case) in future orbits in conjunction with the geosynchronous satellites will unveil spatio-temporal relationships between fields and particles comprehensively.

Acknowledgments. The authors thank the THEMIS team and the LANL EP team for the precious data. We are also grateful to NASA for providing the geosynchronous data through CDAWeb. THEMIS was made possible and is supported in the US by NASA NAS5-02099. This work was partly supported by a JSPS Research Fellowship for Young Scientists 19·1222.

References

Auster, H. U., et al. (2008), The THEMIS Fluxgate Magnetometer, *Space Sci. Rev.* in press.

Belian, R. D., G. R. Gisler, T. Cayton, and R. Christensen (1992), High Z energetic particles at geosynchronous orbit during the great solar proton event of October 1989, *J. Geophys. Res.*, *97*, 16,897.

Belian, R. D., T. E. Cayton, and G. D. Reeves (1995), Quasi-periodic global substorm generated flux variations observed at geosynchronous orbit, *Space Plasmas: Coupling Between Small and Medium Scale Processes, Geophys. Monogr. Ser.*, vol. 86, edited by M. Ashour-Abdalla, T. Chang, and P. Dusenbery, pp.143, AGU, Washington, D. C.

Bonnell, J., et al. (2008), The THEMIS Electric Field Instrument, *Space Sci. Rev.* in press.

Borovsky, J. E., R. J. Nemzek, C. W. Smith, R. M. Skoug, and C. R. Clauer (2003), The solar-wind driving of periodic substorms and global sawtooth oscillations: What determines the periodicity?, *Rep. LAUR-03-8368*, Los Alamos Natl. Lab., Los Alamos, N. M.

Cai, X., M. G. Henderson, and C. R. Clauer (2006), A statistical study of magnetic dipolarization for sawtooth events and isolated substorms at geosynchronous orbit with GOES data, *Ann. Geophys.*, *24*, 3481-3490.

Clauer, C. R., X. Cai, D. Welling, A. DeJong, and M. G. Henderson (2006), Characterizing the 18 April 2002 storm-time sawtooth events using ground magnetic data, *J. Geophys. Res., 111*, A04S90, doi:10.1029/2005JA011099.

Birn, J., M. F. Thomsen, J. E. Borovsky, G. D. Reeves, D. J. McComas, and R. D. Belian (1997), Characteristic plasma properties during dispersionless substorm injections at geosynchronous orbit, *J. Geophys. Res.*, *102(A2)*, 2309-2324.

Henderson, M. G., G. D. Reeves, R. Skoug, M. F. Thomsen, M. H. Denton, S. B. Mende, T. J. Immel, P. C. Brandt, and H. J. Singer (2006a), Magnetospheric and auroral activity during the 18 April 2002 sawtooth event, *J. Geophys. Res.*, *111*, A01S90, doi:10.1029/2005JA011111.

Henderson, M. G., R. Skoug, E. Donovan, M. F. Thomsen, G. D. Reeves, M. H. Denton, H. J. Singer, R. L. McPherron, S. B. Mende, T. J. Immel, J. B. Sigwarth, and L A. Frank (2006b), Substorms during the 10-11 August 2000 sawtooth event, *J. Geophys. Res.*, *111*, A06206, doi:10.1029/2005JA011366.

Huang, C.-S., G. D. Reeves, J. E. Borovsky, R. M. Skoug, Z. Y. Pu, and G. Le (2003a), Periodic magnetospheric substorms and their relationship with solar wind variations, *J. Geophys. Res.*, *108(A6)*, 1255, doi:10.1029/2002JA009704.

Huang, C.-S., J. C. Foster, G. D. Reeves, G. Le, H. U. Frey, C. J. Pollock, and J. M. Jahn (2003b), Periodic magnetospheric substorms: Multiple space-based and ground-based instrumental observations, *J. Geophys. Res.*, *108(A6)*, 1411, doi:10.1029/2003JA009992.

Kitamura, K., H. Kawano, S. Ohtani, A. Yoshikawa, and K. Yumoto (2005), Local time distribution of low and middle latitude ground magnetic disturbances at sawtooth injections of 18-19 April 2002, *J. Geophys. Res.*, *110*, A07208, doi:10.1029/2004JA010734.

Larson, D., et al. (2008), The THEMIS Solid State Telescope, *Space Sci. Rev.*, in press.

Lee, D.-Y., L. R. Lyons, and K. Yumoto (2004), Sawtooth oscillations directly driven by solar wind dynamic pressure enhancements, *J. Geophys. Res.*, *109*, A04202, doi:10.1029/2003JA010246.

McFadden, J. P., et al. (2008), The THEMIS ESA electrostatic analyzer and in-flight calibration, *Space Sci. Rev.* in press.

Mende, S. B., et al. (2008), The THEMIS array of ground based observatories for the study of auroral substorms, *Space Sci. Rev.* in press.

Pulkkinen, T. I., N. Y. Ganushkina, E. I. Tanskanen, M. Kubyshkina, G. D. Reeves, M. F. Thomsen, C. T. Russell, H. J. Singer, J. A. Slavin, and J. Gjerloev (2006), Magnetospheric current systems during stormtime sawtooth events, *J. Geophys. Res., 111*, A11S17, doi:10.1029/2006JA011627.

Tsyganenko, N. A. (2002a), A model of the near magnetosphere with a dawn-dusk asymmetry 1. Mathematical structure, *J. Geophys. Res., 107(A8)*, 1179, doi:10.1029/2001JA000219.

Tsyganenko, N. A. (2002b), A model of the near magnetosphere with a dawn-dusk asymmetry 2. Parameterization and fitting to observations, *J. Geophys. Res., 107(A8)*, 1176, doi:10.1029/2001JA000220.

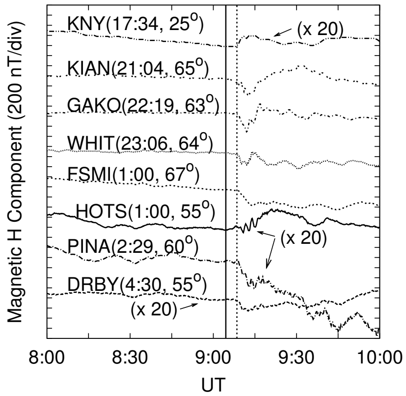

Figure 1. Variations of the magnetic H component observed at the ground stations. The station names, their MLTs at 09:08:30 UT, and CGM latitudes are shown. The magnetic field of Kanoya (KNY), Hot Springs (HOTS), Pinawa (PINA), and Derby (DRBY) are zoomed by 20 for visibility. The solid and dotted vertical lines represent the substorm onset time of 09:04:30 UT and intensification time of 09:08:30 UT, respectively.

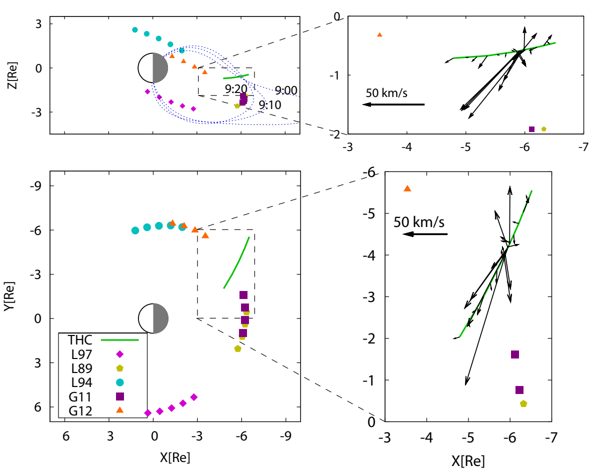

Figure 2. Orbits of the satellites in GSM coordinates from 08:00 UT to 10:00 UT on 20 November 2007. THEMIS-C was outbound. Right panels are enlargements of the THEMIS-C orbit, with ion flows shown by arrows. Blue dotted lines in the upper left panel indicate the model field lines on which THEMIS-C was located at each time.

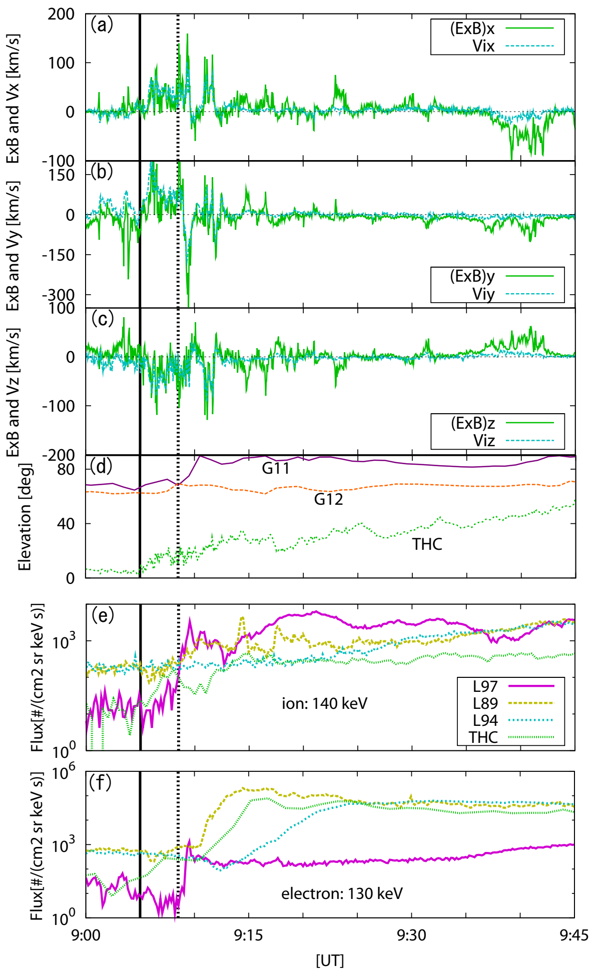

Figure 3. (a-c) Three components of the E×B velocity and the ion velocity perpendicular to the ambient magnetic field. (d) Elevation angle of the magnetic field. (e and f) Energetic proton and electron fluxes. The initiation of the first dipolarization (09:05:00 UT) and the intensification (09:08:30 UT) are indicated by the solid and dotted black lines, respectively.

Table 1. Summary of the observations around the substorm intensification at ~09:08:30 UT. "$(\mathbf{E}\times\mathbf{B})_{\rm in}$" denotes inward convective flows. The circles and crosses indicate "observed" and "not observed", respectively. Hyphen means "not available". The triangles of THC and L94 mean the flux enhancements are rather energy-dispersive. Note that ground stations observed positive/negative bays from 17.5 hours to 4.5 hours MLT.

Satellite (MLT)	dipolarization	$(\mathbf{E}\times\mathbf{B})_{\rm in}$	ions (140 keV)	electrons (130 keV)
L97 (19 h)	$\circ$	-	$\circ$	$\times$
L89 (0 h)	-	-	$\circ$	$\circ$
G11 (0.5 h)	$\circ$	-	-	-
THC (2.5 h)	$\circ$	$\circ$	$\times$	$\triangle$
G12 (4.5 h)	$\circ$	-	-	-
L94 (6 h)	-	-	$\times$	$\triangle$